Journal of the Korean Ceramic Society
Vol. 42, No. 8, pp. 537~541, 2005.

Characterization of Subsurface Damage in Si_3N_4 Ceramics with Static and Dynamic Indentation

Jong Ho Kim,† Young Gu Kim,* and Do Kyung Kim

Department of Materials Science and Engineering, Korea Advanced Institute of Science and Technology, Daejeon 305-701, Korea

(Received July 15, 2005; Accepted July 25, 2005)

ABSTRACT

Silicon nitride is one of the most successful engineering ceramics, owing to a favorable combination of properties, including high strength, high hardness, low thermal expansion coefficient, and high fracture toughness. However, the impact damage behavior of Si_3N_4 ceramics has not been widely characterized. In this study, sphere and explosive indentations were used to characterize the static and dynamic damage behavior of Si_3N_4 ceramics with different microstructures. Three grades of Si_3N_4 with different grain size and shape, fine-equiaxed, medium, and coarse-elongated, were prepared. In order to observe the subsurface damaged zone, a bonded-interface technique was adopted. Subsurface damage evolution of the specimens was then characterized extensively using optical and electron microscopy. It was found that the damage response depends strongly on the microstructure of the ceramics, particularly on the glassy grain boundary phase. In the case of static indentation, examination of subsurface damage revealed competition between brittle and ductile damage modes. In contrast to static indentation results, dynamic indentation induces a massive subsurface yield zone that contains severe micro-failures. In this study, it is suggested that the weak glassy grain boundary phase plays an important role in the resistance to dynamic fracture.

Key words*: *Ceramics, Indentation, Damages, Silicon nitride, Dynamic fracture

1. Introduction

Silicon nitride has received much attention for structural applications, particularly in relation to cutting tools, bearings, and gas turbine engine components.[1] According to early studies ceramics materials, because of their brittleness, are limited in terms of their applicability in structural parts. In the past two decades, silicon nitride has been studied from the viewpoint of microstructural tailoring, and as a result great improvements in its mechanical properties have been achieved.[1] Development and utilization of structural ceramics have required understanding of mechanical properties at a microstructural level. The Hertzian indentation method is one of the preferred methodologies to characterize the elastic and quasi-plastic properties of ceramics.[2] Lee's work on indentation on various silicon nitrides has elucidated the microstructural effects on mechanical properties; especially flexural strength, yield strength, and R-curve behavior.[3] Also, numerous studies have attempted to improve the mechanical properties through the design of microstructure.[3]

Whereas silicon carbide is a potential candidate for ceramic or ceramic composite armor systems, silicon nitride has not been successfully applied to armor systems. Recently, newly developed silicon nitrides have comparably high hardness, toughness, and modulus, relative to those of silicon carbide, and thus it is expected that silicon nitride could provide effective resistance to dynamic fracture. Dynamic damage evolution of silicon carbide has been extensively studied and Meyers presented a sound explanation of the dynamic deformation of silicon carbide.[4] However, relatively few studies have been devoted to the dynamic fracture behavior of silicon nitride ceramics. Previous studies have provided evidence of an interrelationship between the static and dynamic indentation properties of silicon carbides and nitrides.[5-8]

In this study, we conduct static and dynamic indentation experiments on three grades of silicon nitrides. Static mechanical properties were derived from sphere indentation and dynamic fracture phenomena were observed carefully to determine the dynamic deformation mode in silicon nitrides. Subsurface damage of each specimen with static and dynamic indentation was characterized using a bonded-interface technique. In order to elucidate the resistance to ballistic impact, a two-dimensional finite element analysis was conducted to simulate the projectile penetration and determine the ballistic efficiency.

2. Experimental Procedure

The starting silicon nitride powder (α-Si_3N_4 UBE-SN-E10, Ube Industries, Tokyo, Japan) with additives has the fol-

†Corresponding author : Jong Ho Kim
E-mail : darkstar12@kaist.ac.kr
Tel : +82-42-869-4151 Fax : +82-42-869-3310
*Current address : Samsung Electronics

lowing composition: 5 wt% Y_2O_3 (Fine Grade H. C. Starck GmBH, Goslar, Germany), 2 wt% Al_2O_3 (AKP50, Sumitomo Chem. Co. Ltd. Tokyo, Japan), and 1 wt% MgO (High Purity Baikowski Co. NC. USA). The powder was mixed as a slurry in isopropanol for 24 h in a planetary zirconia ball mill in a propylene container. After drying, the agglomerated powder was crushed and sieved with a 120 mesh screen. Consolidation was achieved in nitrogen gas at 1 atm under a uniaxial pressure of 25 MPa, at 1600, 1700, and 1800°C for 1 h in a hot press (Astro Industries Inc., USA). These sintering temperatures respectively produced fine equiaxed (F), medium (M), and coarse elongated (C) microstructure.

Specimen surfaces normal to the hot pressing direction were polished to 1 μm finish so as to enable optical microscopy observation. The surfaces were then plasma etched to reveal the grain structures. The microstructures of the specimens were observed by Scanning Electron Microscopy (SEM XL30, Philips Netherlands). Fig. 1 shows SEM images of the specimens. Silicon nitrides have bimodal structures with a different ratio of α and β: F-Si_3N_4 with ~75% 0.5 μm α grains and ~15% β grains, M-Si_3N_4 with ~78% 0.5 μm wide and 4 μm grains and ~12% α grains, C-Si_3N_4 with 100% 1.5 μm wide and 9.0 μm long β grains.

Table 1 shows the basic physical properties of the three silicon nitride specimens. The density of the specimens was determined by the Archimedes method and it was confirmed that the specimens were near full dense. Young's modulus and Poisson's ratio were determined for each specimen using the routine impulse excitation technique.[9] Vickers indentations were used to determine the hardness of the specimens. In order to determine the specimen strength, flexure tests were conducted in four-point bending with 5 × 3 × 30 mm samples. Another set of bend tests was made on specimens after Vickers indentation to estimate the toughness.[10] M-Si_3N_4 specimens display the highest strength value and the hardness of F-Si_3N_4 is higher than that of the other specimens. Of particular interest is the R-curve behavior observed in C-Si_3N_4, which has higher toughness than other specimens.

Hertzian indentation tests were conducted to observe the evolution of damage in each specimen. The detailed procedure of specimen preparation for subsurface observation can be found elsewhere.[11] In the preparation of the bonded specimen, the gaps between two bars were maintained below 10 μm so as to minimize additional free surface effects. With this sample preparation method, fracture and deformation features induced by shear stress were not evident; however, testing with a shallow free surface offers qualitative information on the failure mechanism in ceramic materials. After Hertzian indentation testing, the specimens were separated and their side surfaces were gold coated for viewing under a Nomarski interference optical microscope and SEM. Using the indentation stress-strain relationship, the brittle and quasi-plastic region can be separated by the transition point, and the yield strength and strain hardening coefficient were determined.

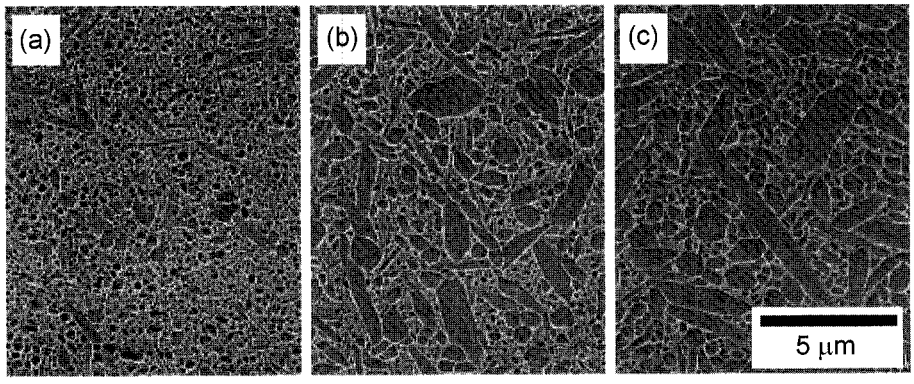

Fig. 1. SEM micrographs of polished and plasma-etched silicon nitride specimens; (a) F-Si_3N_4, (b) M-Si_3N_4, and (c) C-Si_3N_4.

Table 1. Processing and Physical Properties of Silicon Nitrides

Material	F-Si_3N_4	M-Si_3N_4	C-Si_3N_4
Processing condition	Hot-press at 1600°C	Hot-press at 1700°C	Hot-press at 1800°C
Hardness, H (GPa)	20.6	16.5	15.9
Toughness, T (MPa $m^{1/2}$)	3.8	5.3	4.9-7.3†
Strength, σ_F (MPa)	885	1084	792
Young's modulus, E (GPa)	331	326	314
Poisson's ration, υ	0.27	0.28	0.29
Yield stress, Y (GPa)¶	11.7	9.5	7.2
Strain hardening coefficient¶	1	0.7	0.5

†R-curve behavior is observed, ¶Determined by static Hertzian indentation testing and corresponding FEA.

Explosive indentation testing was conducted on the same dimensions of bonded-interface specimens in order to reveal dynamic deformation of the specimens. These specimens were clamped with an auxiliary fixture to inhibit shattering of the specimen during impact loading. Dynamic indentation was performed using an Electric Bridge Wire (EBW) detonator. The small explosive detonator was encased in a stainless steel cylinder and a 5 mm diameter bottom plate. The detonator propels the bottom stainless steel flyer to generate impact shock compression.

3. Results and Discussion

3.1. Static and Dynamic Indentation Damage

The subsurface damages of each sphere-indented silicon nitride are shown in Fig. 2(a), (b), and (c). A principal advantage of the Hertzian indentation method is its capacity to reveal fundamental deformation-fracture properties in a highly controlled manner. Observed damage patterns show general trends of microstructure tailored silicon nitride. An apparent transition from brittle fracture to quasi-plastic damage behavior is observed through the F→M→C series. This transition to quasi-plasticity occurs with increasing heterogeneity of the microstructure and long crack toughness. As seen in Fig. 2(a), (b), and (c), cone cracking is dominant in the high hardness specimens (F), and quasi-plasticity in the high toughness specimens (C). The M-Si_3N_4 specimen shows a combination of cone cracking and quasi-plasticity.

Sub-surface side views of explosively indented specimens are shown in the lower series micrographs of Fig. 2. As seen in the micrographs, radial and lateral cracks are distributed throughout the specimen with fragmentation and spallation. The macroscopic cracking and spallation appear to represent post-shock damage, because the reflected wave breaks the specimen into several pieces. This can be inferred from the observation that the orientation of the macroscopic cracks corresponds precisely with the normal of the compressive wave. In contrast to sphere indentation, brittle to quasi-plastic transition is not clearly shown. However, spall-dominant fracture in quasiplastic damage mode is apparent in a sequence of F→M→C. Interestingly, the F-Si_3N_4 specimen has a quasi-plastic deformation zone just below the spallation region. This implies that all specimens would display quasi-plastic deformation. In our previous study on silicon carbide, the effectiveness of the weak grain boundary phase on the evolution of subsurface damage with explosive indentation was reported.[8] Based on the same mechanism, a grain boundary glassy phase on the entire grain boundary surface appears to induce quasi-plastic deformation. During dynamic compression, the weak glassy grain boundary tends to slide and fail easily. The same failure mechanism, attacking a weak grain boundary, was also noted by Shih et al. and Lundberg et al. with regard to the dynamic failure of some ceramics.[4,12] Silicon nitrides have a relatively small grain size and this affects the formation of shear faults, resulting in relatively small crack size inside the quasi-plastic zone.

The damaged silicon nitride specimens were examined via optical microscopy and extensive SEM work was conducted on the quasi-plastic zone to determine the fracture mode during dynamic fracture of silicon nitride. In Fig. 3(a), crack deflection and bridging behavior were observed in the macro-cracked region. Systematic examination of the quasi-plastic deformation zone revealed strong evidence of grain boundary attacking and trangranular fracture mode in silicon nitride. Two fracture modes can be explained in the same manner, as suggested by Meyers's principal damage initiation mechanism.[4] In Fig. 3(b) and (e), grain boundary debonding and voids initiation is the dominant fracture

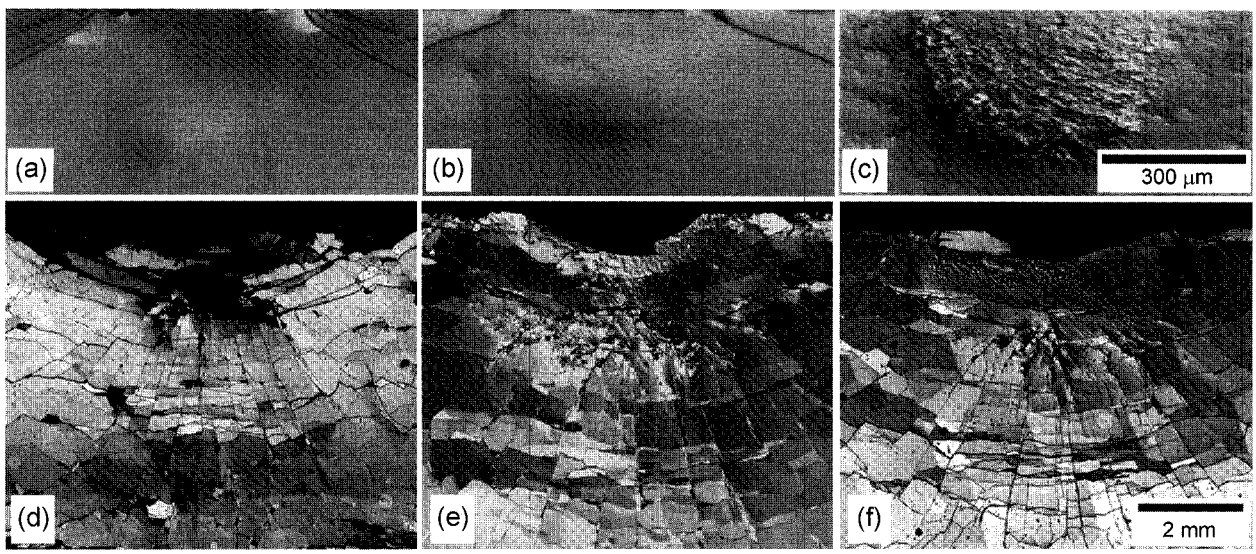

Fig. 2. Static Hertzian indentation damage of Si_3N_4; (a) F-Si_3N_4, (b) M-Si_3N_4, (c) C-Si_3N_4 and explosive indentation damage of specimens; (d) F-Si_3N_4, (e) M-Si_3N_4, (f) C-Si_3N_4.

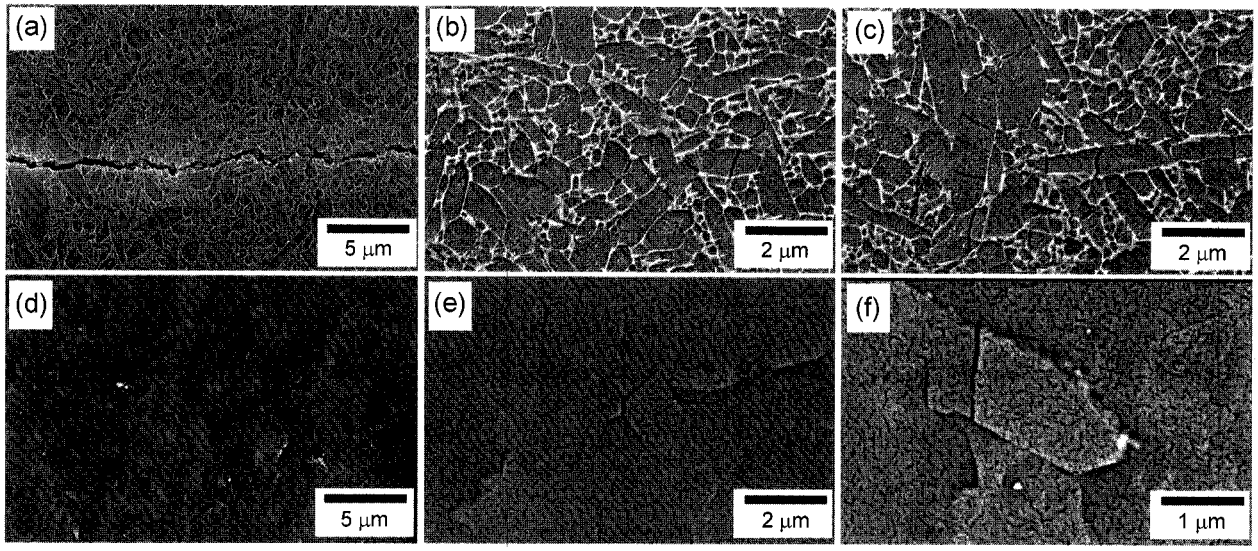

Fig. 3. SEM micrographs of quasi-plastic deformation zone, SE; (a) macrocrack, (b) intergranular failure, (c) trans and intergranular failure and BSE images of (d) deformation zone, (e) intergranular failure, (f) trans and intergranular failure.

mode and in Fig. 3(c) and (f), an elongated abnormal grain breaks into several parts. Two mixed fracture modes in the quasi-plastic zone are mainly due to the glassy grain boundary phase and display trends corresponding with comminuted zone of impact damaged SiC in Hauver *et al.*'s work.[13]

3.2. Ballistic Efficiency of Silicon Nitride Ceramics

A two-dimensional explicit time integration finite element code of Lagrangian description was used to simulate the dynamic brittle fracture of ceramics.[14] In this code, when the traction is greater than the critical spall strength, tensile cracks can grow. These cracks can branch, coalesce, and eventually lead to fragmentation. Dynamic compressive load induced plastic deformation was integrated in this code. In the numerical calculation, it is assumed that a 7.6 mm hard steel projectile with 830 m/s speed strikes a ceramic tile on an aluminum plate. An axisymmetric model was used and calculation parameters were adopted from the physical properties and static indentation results. Evolution of cracking and spalling was monitored as the time scale and final penetration depth were measured.

Fig. 4(a) shows a screenshot of a typical simulation of residual penetration of a projectile into 3.0 mm thick M-Si_3N_4 on an aluminum backing. The ceramic tile was comminuted at an early stage, followed by penetration of the projectile into the aluminum. The residual projectile had a slightly eroded tip and its shape was sustained during penetration. Of particular importance in this calculation is that all input data was adopted from the physical properties and sphere indentation results. Thus, a combination of finite element analysis code and sphere indentation facilitates prediction of the effectiveness of armor ceramics.

In order to calculate the ballistic efficiency, the axes of penetration versus tile thickness were normalized by multiplying them by the corresponding densities of aluminum and ceramic; thus, the slope of the fit line corresponds to the

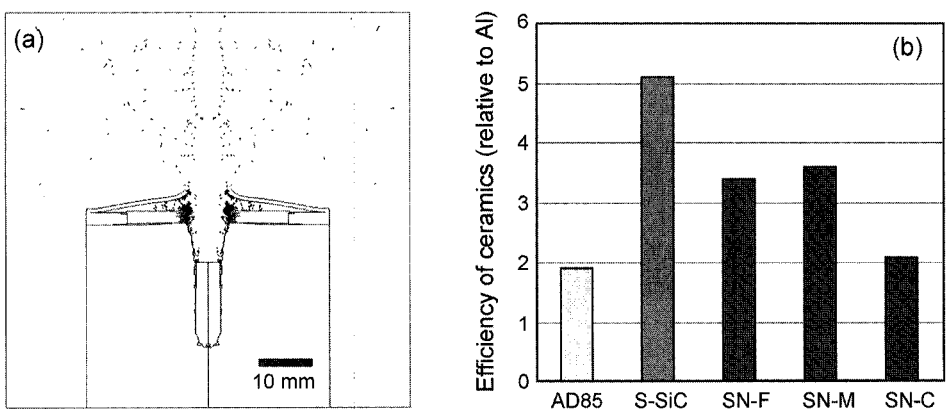

Fig. 4. Simulation of depth-of-penetration test with 3 mm thick ceramics and aluminum backing hit by 7 mm diameter hard steel projectile; (a) M-Si_3N_4 ceramics (SN-M) result and (b) efficiency of silicon nitride ceramics with a comparison of alumina and sintered SiC ceramics.

ballistic efficiency. Alumina AD85 and SiC are the most well-known armor ceramic materials and their ballistic efficiency values have been reported by Rozenberg and Yeshurun.[15] Calculated efficiencies of alumina and SiC ceramics in this study show slightly lower values than the published data, but show good agreement in terms of trend. The efficiency of silicon nitrides lies between that of SiC and AD85 alumina, ranging from 2 to 4. Fine and medium grain shaped silicon nitride shows 3.5 efficiency whereas the coarse grained silicon nitride displays the lowest efficiency values, approximately 2. Silicon nitride has comparable values of hardness, strength, and toughness to silicon carbide but its ballistic efficiency is lower than that of solid-state-sintered SiC. The relatively low values of efficiency of Si3N4 ceramics may be related to the existence of a glassy grain boundary phase, which is a source of compressive-driven faults. Grain coarsening also appears to be a source of decline in the ballistic resistance of ceramics, as seen in C-Si_3N_4. In ceramics with a grain boundary phase, the primary failure mode with dynamic impact is quasi-plastic deformation induced by high compressive stress. In dynamic indentation as well static Hertzian indentation testing, C-Si_3N_4 displays a quasi-plastic damage mode with shear faults and clouds of micro-cracks. The superior M-Si_3N_4 efficiency might result from an appropriate combination of physical properties, such as high hardness, high strength, etc.

4. Conclusions

Sphere and explosive indentation testing on hot-pressed silicon nitrides were used to study the effects of microstructure. Silicon nitrides displayed brittle fracture behavior in fine grained specimens and quasi-plastic deformation in coarse grained specimens with static sphere indentation. In contrast to static indentation, upon explosive indentation, quasi-plastic damage mode was the primary failure mode in all microstructure of silicon nitride. Extensive scanning electron microscopy observations in the region of the damaged subsurface quasi-plastic zone confirmed the nature of the dynamic fracture mode: grain boundary attacking and transgranular cracking. The weakness of the glassy grain boundary phase in silicon nitride ceramics is considered one of the important factors in determining ballistic efficiency. Microstructure control of silicon nitride could optimize the dynamic mechanical properties for development of successful armor applications.

REFERENCES

1. P. F. Becher, S. L. Hwang, H. T. Lin, and T. N. Tiegs, "Tailoring of Mechanical Properties of Si_3N_4 Ceramics," Kluwer Academic Publishers (1994).
2. B. R. Lawn, "Indentation of Ceramics with Spheres : A Century after Hertz," *J. Am. Ceram. Soc.*, **81** [8] 1977-94 (1998).
3. S. K. Lee, K. S. Lee, B. R. Lawn, and D. K. Kim, "Effect of Starting Powder on Damage Resistance of Silicon Nitrides," *J. Am. Ceram. Soc.*, **81** [8] 2061-70 (1998).
4. C. J. Shih, M. A. Meyers, V. F. Nesterenko, and S. J. Chen, "Damage Evolution in Dynamic Deformation of Silicon Carbide," *Acta Mater.*, **48** [6] 2399-420 (2000).
5. D. K. Kim and C.-S. Lee, "Indentation Damage Behavior of Armor Ceramics," *Proc of the Symposium on Ceramic Armor Materials by Design*, **PAC RIM 4** 429-40 (2001).
6. D. K. Kim, C.-S. Lee, and Y.-G. Kim, "Dynamic Indentation Damage of Ceramcis," *Proc of the Symposium on Ceramic Armor Materials by Design*, **PAC RIM 4** 261-69 (2001).
7. D. K. Kim, J. H. Kim, Y.-G. Kim, C.-S. Lee, D.-T. Chung, C. W. Kim, J. H. Choi, and S.-N. Chang, "Controlled Explosive Indentation on Ceramics," *Proc of the Ceramic Armor and Armor Systems Symposium, Annual Meeting of American Ceramic Society*, 93-104 (2003).
8. J. H. Kim, Y.-G. Kim, D. K. Kim, K. S. Lee, and S.-N. Chang, "Static and Dynamic Indentation Damage in SiC and Si_3N_4," *Key Eng. Mater.*, **287** [5] 410-15 (2004).
9. "Standard Test Method for Dynamic Young's Modulus, Shear Modulus, and Poisson's Ratio for Advanced Ceramics by Impulse Excitation of Vibration," *ASTM* **C1259-01** (2001).
10. G. R. Antis, P. Chantikul, D. B. Marshall, and B. R. Lawn, "A Critical Evaluation of Indentation Technique for Measuring Fracture Toughness," *J. Am Ceram. Soc.*, **64** [9] 533-38 (1981).
11. F. Guiberteau, N. P. Padture, and B. R. Lawn, "Effect of Grain Size on Hertzian Contact Damage in Al_2O_3," *J. Am. Ceram. Soc.*, **77** [7] 1825-31 (1994).
12. P. Lundberg, R. Renstrom, and B. Lundberg, "Impact of Metallic Projectiles on Ceramic Targets : Transition between Interface Defeat and Penetration," *Int. J. Impact Eng.*, **24** [3] 259-75 (2000).
13. G. E. Hauver, P. H. Netherwood, R. F. Bench, and L. J. Kecskes, *Proc 19th Army Symp. Solid Mech.*, Orlando, FL USA (1994).
14. D. T. Chung, C. Hwang, S. I. Oh, and Y. H. Yoo, "A Study on the Dynamic Brittle Fracture Simulation," *The 4th Int. Symp. on Impact Eng.*, 16-8, Kumamoto, Japan (2001).
15. Z. Rozenberg and Y. Yeshurun, "The Relation between Ballistic Efficiency and Compressive Strength of Ceramic Tiles," *Int. J. Impact Eng.*, **7** 357-62 (1988).